Nonaggregating Mutant of Recombinant Human Hexokinase I Exhibits Wild-Type Kinetics and Rod-like Conformations in Solution†

Alexander E. Aleshin,‡ Marc Malfois,§ Xiaofang Liu,‡ Chang Sup Kim,‡ Herbert J. Fromm,‡ Richard B. Honzatko,*,‡ Michel H. J. Koch,§ and Dmitri I. Svergun*,§,||

Department of Biochemistry, Biophysics and Molecular Biology, Iowa State University, Ames, Iowa 50011, and European Molecular Biology Laboratory, Hamburg Outstation, EMBL c/o DESY, Notkestrasse 85, D-22603 Hamburg, Germany, and Institute of Crystallography, Russian Academy of Sciences, 117333 Moscow, Russia

Received March 4, 1999; Revised Manuscript Received April 29, 1999

ABSTRACT: Hexokinase I governs the rate-limiting step of glycolysis in brain tissue, being inhibited by its product, glucose 6-phosphate, and allosterically relieved of product inhibition by phosphate. On the basis of small-angle X-ray scattering, the wild-type enzyme is a monomer in the presence of glucose and phosphate at protein concentrations up to 10 mg/mL, but in the presence of glucose 6-phosphate, is a dimer down to protein concentrations as low as 1 mg/mL. A mutant form of hexokinase I, specifically engineered by directed mutation to block dimerization, remains monomeric at high protein concentration under all conditions of ligation. This nondimerizing mutant exhibits wild-type activity, potent inhibition by glucose 6-phosphate, and phosphate reversal of product inhibition. Small-angle X-ray scattering data from the mutant hexokinase I in the presence of glucose/phosphate, glucose/glucose 6-phosphate, and glucose/ADP/Mg^{2+}/AlF_3 are consistent with a rodlike conformation for the monomer similar to that observed in crystal structures of the hexokinase I dimer. Hence, any mechanism for allosteric regulation of hexokinase I should maintain a global conformation of the polypeptide similar to that observed in crystallographic structures.

Hexokinase I (ATP: D-hexose 6-phosphotransferase, EC 2.7.1.1) governs the flow of glucose into the energy metabolism of brain tissue and red blood cells (*1*). The type I isozyme [one of four isozymes found in mammals (*2*)] consists of a single polypeptide of molecular mass 100 kDa, which shows 50% sequence identity between its N- and C-terminal halves (*3*, *4*). The sequence identity putatively is a consequence of duplication and fusion of a primordial hexokinase gene (*5*−*8*). Hexokinase I uses ATP to phosphorylate the 6-hydroxyl group of glucose and is inhibited potently by the product, glucose 6-phosphate (Glc-6-P).[1] Hexokinase I is distinct from isozymes II−IV in that inorganic phosphate (P_i) at physiological levels can relieve inhibition by Glc-6-P (*9*−*11*).

At low concentrations (below 10 μg/mL of enzyme) typical for kinetics investigations, hexokinase I is putatively a monomer (*12*). At elevated concentrations (above 10 mg/mL), hexokinase I aggregates and appears as a dimer in all crystallographic structures (*13*−*16*). The extent to which dimerization of hexokinase I perturbs the conformation of the monomer is unclear. Crystallographic dimers have hinge elements which permit rigid-body movements of structural domains within the N- and C-terminal halves. More significantly, the long transition helix between the two halves of a monomer has the propensity to bend and/or reorient (*13*, *16*). A bent or reoriented transition helix could allow a monomer to adopt a radically different conformation in solution, in which the N-terminal half of hexokinase I establishes an extensive new interface with the C-terminal half. The new interface would involve elements of the active site of the C-terminal half. Hence, in order to develop a correct model for allosteric regulation in monomeric hexokinase I, the limits of conformational change in the monomer under various states of ligation must be defined with greater certainty.

Unfortunately, experimental methods currently available to probe macromolecular conformation have in common a requirement for high protein concentration in solution. In the case of hexokinase I, the enzyme concentrations necessary for the growth of crystals, and for experiments in NMR and light scattering, creates in solution a mixture of dimers and monomers of the wild-type enzyme. Reported below are the properties of a mutant hexokinase I, in which residues critical to the stability of the dimer have been changed by directed mutation. On the basis of small-angle X-ray scattering data, the resulting mutant exists in solution as a monomer at elevated concentrations of enzyme, either in the

† This work was supported in part by National Institutes of Health Research Grant NS 10546, National Science Foundation Grants MCB-9603595 and MCB-9316244, and European Union Biotechnology Program, Grant BIO4-CT97-2143 (to D.I.S.). This is journal paper J-18339 of the Iowa Agriculture and Home Economics Experiment Station, Ames, Project 3191, and supported by the Hatch Act and State of Iowa funds.

* To whom correspondence should be addressed. (R.B.H.) Phone: 515-294-6116. Fax: 515-294-0453. E-mail: honzatko@iastate.edu. (D.I.S.) Phone: +4940899020. Fax: +494089902149. E-mail: svergun@embl-hamburg.de.

‡ Iowa State University.

§ European Molecular Biology Laboratory.

|| Institute of Crystallography, Russian Academy of Sciences.

[1] Abbreviations: Glc-6-P, glucose 6-phosphate, 1,5-AnG-6-P, 1,5-anhydroglucitol 6-phosphate; P_i, inorganic phosphate; Glc, glucose; WT, wild-type; PDB, Protein Data Bank at Brookhaven National Laboratory.

10.1021/bi990523n CCC: $18.00
Published on Web 06/06/1999

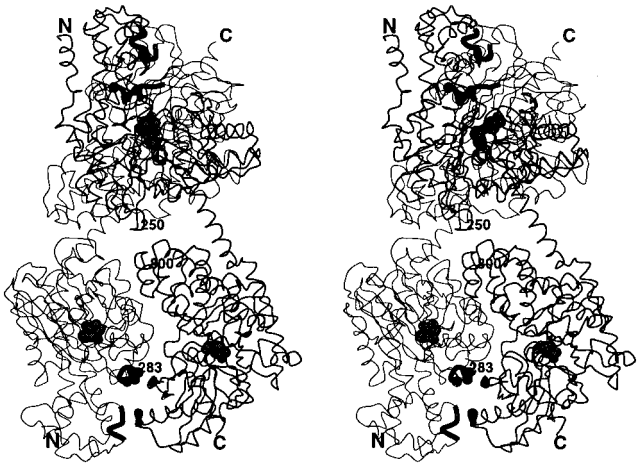

FIGURE 1: Sterreoview of the 1−6 interface of the hexokinase I dimer. Two polypeptide chains are represented in different line widths. The main-chain elements of residues, which contribute nonbonded contacts to the 1−6 interface, are in bold lines with black dots representing the positions of mutated residues. Residues 242−250 of the N-terminal half and 796−813 of the C-terminal half may be important to the allosteric mechanism of hexokinase I. Glucose molecules (space filling representation) at the N- and C-terminal halves mark the approximate locations of allosteric and active sites, respectively. The image is drawn with MOLSCRIPT (*34*).

presence or absence of ligands. Furthermore, this nonaggregating form of hexokinase I has kinetic properties nearly identical to those of the wild-type enzyme. Under all conditions of ligation explored here, the nonaggregating mutant has a rodlike conformation in solution, which is similar to that observed for a single polypeptide chain of the crystalline dimer. Hence, allosteric regulation of catalysis in monomeric hexokinase I probably involves an interface between the N- and C-terminal halves, similar to ones currently defined by crystal structures.

MATERIALS AND METHODS

Materials. A full-length cDNA of human brain hexokinase, cloned into an expression vector pET-11a (from Novagen) to produce pET-11a-HKI, was available from a previous study (*17*). The Transformer Site-Directed Mutagenesis Kit is from Clontech Laboratories, Inc. T4 polynucleotide kinase, T4 DNA ligase, plasmid pGEM-7Z(+), the Magic Miniprep DNA purification system, and restriction enzymes were from Promega. Oligonucleotide synthesis and DNA sequencing were done at the Iowa State University Nucleic Acid Facility. *Escherichia coli* strain ZSC13, which does not contain endogenous hexokinase, was a gift from the Genetic Stock Center, Yale University. ATP, NADP, streptomycin sulfate, 1,5-anhydro-D-sorbitol, deoxyribonuclease I (DNAase I), leupeptin, phenylmethanesulfonyl fluoride (PMSF), and ampicillin were from Sigma. Glucose-6-phosphate dehydrogenase came from Boehringer Mannheim. Isopropyl-1-thio-β-D-galactopyranoside (IPTG) was from BioWorld. Bio-gel hydroxapatite came from Bio-Rad and DEAE-Toyopearl 650M resin was from TosoHass.

Rationale for Mutations. The critical interactions which putatively stabilize crystallographic dimers of hexokinase I are at the 1−6 interface (Figure 1). The 1−6 interface is preserved in two conformational states of the dimer, which differ significantly from each other (*13, 14*). Glu280, Arg283, and Gly284 are at the 1−6 interface in crystallographic dimers and yet are remote from known ligand binding sites of the N-terminal half and from the interface between N- and C-terminal halves within a monomer. The mutation of Glu280 and Arg283 to alanine eliminates hydrogen bonds between monomers of crystallographic dimers and the mutation of Gly284 to tyrosine introduces steric hindrance. The main chain angles ($\varphi = -113°$, $\psi = 2°$) and the structural context of Gly284 permit the introduction of a tyrosyl side chain, which would project out from the surface of the protein.

Construction of Mutant Hexokinase Genes. Mutagenesis was performed according to protocols provided with the Transformer Site-Directed Mutagenesis Kit, except that alkaline denaturation/ethanol precipitation was employed to produce single-strand plasmids instead of heat denaturation. The triple mutation, ($Glu^{280} \rightarrow Ala/Arg^{283} \rightarrow Ala/Gly^{284} \rightarrow Tyr$), was introduced by means of an oligonucleotide of the following sequence:

5′-CAGAGTTTGACAGG**GCA**ATTGAC**GCATAT**TCC-CTCAACCCTGG- 3′ where altered codons are in boldface type. The primer used for selection, 5′-GAGCCTCGC**CTC-GAG**AACGCCAGCAAG-3′, converts the unique *Nru*I site to another unique *Xho*I site. The mutation was confirmed by sequencing the entire insert by the fluorescent, dideoxy chain termination method (Iowa State University DNA Facility).

Expression and Purification of Wild-Type and Mutant Hexokinase I. Wild-type and mutant forms of hexokinase I were produced by growing pET-11a-HKI-transformed *E. coli* strain ZSC13 overnight in LB medium plus 40 μg/mL ampicillin. The resulting innoculant was added to a 100-fold volume of M9 medium with 100 μg/mL ampicillin. The culture was grown in a fermentor (with stirring of 200 rpm and a filtered air flow of 6 L/min) at 37 °C to early log phase ($A_{600} = 0.4$), after which isopropyl-D-thiogalactopyranoside (IPTG) was added to a final concentration of 0.4 mM to induce the T7 RNA polymerase gene. The culture was grown for an additional 20−24 h at 22 °C. The wild-type and mutant forms of hexokinase I were purified by streptomycin sulfate precipitation, DEAE-anion exchange column chromatography, hydroxyapatite column chromatography, and DEAE 5PW Spherogel TSK-G HPLC chromatography as described elsewhere (*13, 14, 18*). The final step of purification separated the enzyme into two electrophoretically indistinguishable components. The leading fraction, which contained 75% of the total activity, was used in studies reported here.

Measurement of Protein Concentration. Concentrations of wild-type and mutant hexokinases used in kinetics assays were determined by the method of Bradford (*19*), using bovine serum albumin as a standard. Protein concentrations for small-angle scattering experiments were determined spectrophotometrically at a wavelength of 280 nm, using an extinction coefficient of 0.52 mL mg^{-1} cm^{-1}.

Preparation of 1,5-Anhydroglucitol-6-phosphate. The barium salt of 1,5-anhydroglucitol-6-phosphate (1,5-AnG-6-P) was prepared as described elsewhere (*20*). A precisely weighed amount of the barium salt of 1,5-AnG-6-P was dissolved in distilled water by adding HCl. Barium ions were removed

by titration with a stoichiometric amount of 1 M Na_2SO_4 followed by centrifugation.

Hexokinase Assay and Kinetics. Hexokinase activity was determined by the Glucose-6-phosphate dehydrogenase coupled spectrometric assay as described elsewhere (*21*). Mutant and wild-type enzymes were dialyzed against 50 mM Hepes, pH 7.5, just prior to their use in activity assays. Glucose-6-phosphate dehydrogenase was dialyzed exhaustively in order to remove ammonium sulfate. Assays were performed in Hepes/sodium acetate (50 mM/100 mM, pH 7.8). Care was taken to minimize the introduction of phosphate and/or sulfate as contaminants of assay components. Mg^{2+} was added to each assay to a concentration of 2 mM in excess of the ATP concentration. The concentration of hexokinase used for activity assays was 1.2−2.0 μg/mL. The concentrations of 1,5-AnG-6-P used in the determination of K_i and K_{ii} were 0, 100, 200, 300, and 400 μM, at ATP concentrations of 4.0, 2.3, 0.90, 0.60, 0.45, and 0.30 mM. Phosphate relief of product inhibtion employed an ATP concentration of 0.60 mM, P_i concentrations of 3 and 6 mM, and concentrations for 1,5-AnG-6-P as above for the determination of K_i and K_{ii}. Initial rate data were analyzed by using a computer program written in MINITAB language with an α value of 2.0 (*17*). Data representing the relation of reciprocal velocity to concentrations of ATP and 1,5-AnG-6-P were fitted to a kinetic model for nonlinear competitive inhibition:

$$1/v = (1/V_m)[1 + (K_a/A)(1 + I/K_i + I^2/K_iK_{ii})] \quad (1)$$

In the above, v, V_m, and A represent initial velocity, maximum velocity, and ATP concentration, respectively, and K_a, K_i, and K_{ii} represent dissociation constants for ATP, a high affinity binding site for 1,5-AnG-6-P, and a low affinity site for 1,5-AnG-6-P, respectively. Equation 1 and its associated kinetic scheme were presented in previous work (*18*).

Circular Dichroism Measurements. CD spectra were measured from 200 to 260 nm at room temperature from samples of mutant and wild-type hexokinases (protein concentrations of 200 μg/mL in 2.0 mM Hepes, pH 7.5, 0.1 mM glucose, and 0.25 mM β-mercaptoethanol, with and without 1 mM Glc-6-P, using a Jasco J710 CD spectropolarimeter.

Modeling of Monomers. Crystal structures of hexokinase I dimers [PDB accession codes 1HKB (*14*) and 1HKC (*13*)] are points of departure in modeling plausible conformational states of monomeric hexokinase I. The models are used in the calculation of scattering intensities (see below). A single polypeptide chain and the entire dimer of the Glc/Glc-6-P complex [PDB accession code 1HKB (*14*)] were adopted as models for monomers and dimers in solution, respectively. In these models, both the N- and C-terminal halves are in a closed conformation (*14*). Models with open N- and/or C-terminal halves were built by superposition of an open N-terminal half (using its small domain) and/or an open C-terminal half (using its large domain) onto corresponding domains of a single polypeptide chain from the Glc/Glc-6-P complex. Models for open N- and C-terminal halves come from a previous study (*13*).

Other models were developed in order to ascertain the global conformational state of the monomer under different conditions of ligation. Small-angle scattering intensities are sensitive to conformational changes, which alter the gross structure or anisometry. Hence, distinguishable models of the monomer (at the resolution of small-angle scattering data) require repositioning of the N-terminal half relative to the C-terminal half so as to significantly change the global conformation of the polypeptide chain. The calculated scattering intensities are insensitive, however, to the exact details of the conformational change. Hence, we arbitrarily let the axis of the transition helix define the principal direction of the monomer and the Cα atom of residue 475 (which lies at the C-terminal end of the transition helix) be a point of articulation. Fixing the C-terminal half in place, the transition helix and its attached N-terminal half can be reoriented by rotations about an axis perpendicular to the transition helix. Superposition of the N-terminal half of hexokinase I onto the C-terminal half reveals a different orientation of the first helix of the N-terminal half relative to the transition helix. The axes of the transition helix and the first helix of the superimposed N-terminal half define a plane. The rotation axis used to generate models here is perpendicular to this plane.

Small-Angle X-ray Scattering. X-ray scattering data were collected on the EMBL, ×33 camera (*22*−*24*) on the storage ring DORIS III of the Deutsches Elektronen Synchrotron (DESY) using multiwire proportional chambers with delay line readout (*25*). At the sample−detector distance of 3 m and a wavelength λ of 0.15 nm, the sampled range of momentum transfer was $0.1 < s < 2$ nm^{-1} [$s = (4\pi \sin \theta)/\lambda$, where 2θ is the scattering angle]. Scattering intensities were measured from either wild-type or the interface mutant hexokinases (protein concentrations varying from 0.4 to 16 mg/mL) in a buffer containing Hepes (50 mM, pH 7.8), dithiothreitol (2 mM), glucose (1 mM) and β-mercaptoethanol (1 mM) with either (i) Glc-6-P (1 mM)/sodium acetate (100 mM), (ii) P_i (1 mM)/sodium acetate (100 mM), or (iii) ADP (10 mM)/NaCl (100 mM)/$Mg(NO_3)_2$ (20 mM)/NaF (5 mM)/ $Al(NO_3)_3$ (0.5 mM). The data were normalized to the intensity of the incident beam, and corrected for detector response. Scattering due to the buffer was subtracted, and the resulting difference curves were scaled to the enzyme concentration. All procedures involve statistical error propagation using the program SAPOKO (D.I.S. and M.H.J.K., unpublished material).

The forward scattering $I(0)$ and radius of gyration R_g of individual curves were evaluated using the Guinier approximation, $I_{exp}(s) = I(0)\exp(-s^2R_g2/3)$, which is valid for $(sR_g) < 1.3$ (*26*) and also from the entire scattering curve using the indirect transform package GNOM (*27*). The maximum dimensions of the hexokinases were estimated by use of the orthogonal expansion program ORTOGNOM (*28*). The extrapolated forward scattering value $I(0)$ was used to evaluate the molecular mass of the solute after normalization against the reference scattering from solutions of bovine serum albumin.

Scattering curves from models were calculated using the program CRYSOL (*29*), which takes into account the scattering from the solvation shell at the surface of the protein model. The model is covered by a hydration layer of thickness 0.3 nm with an adjustable density ρ_b, which may differ from that of the bulk solvent ρ_s. The scattering from

Table 1: Kinetic Parameters for Wild-Type and Interface-Mutant Hexokinases[a]

kinetic parameter	wild-type hexokinase I[b]	interface mutant hexokinase I[b]
k_{cat} (s^{-1})	100(10)	100(6)
K_m (glucose) (μM)	61(6)	57(5)
K_m (ATP) (mM)	1.2(0.2)	0.66(0.06)
K_i (1,5-AnG-6-P) (μM)	15(2)	23(2)
K_{ii} (1,5-AnG-6-P) (mM)	1.4(0.4)	3(2)
P_i relief[c](%)	72(6)	80(6)

[a] Values in parentheses are standard deviation. [b] K_i and K_{ii} were obtained by fitting data (plots of 1/velocity versus 1/[ATP] at 2 mM glucose with 1,5-AnG-6-P ranging from 0 to 400 μM) to a model for nonlinear competitive inhibition (eq 1). [c] Percent relief of 1,5-AnG-6-P inhibition by P_i was determined as follows: $100 \times (A - B)/A$, where A is the slope from the plot of (relative velocity of hexokinase)$^{-1}$ versus 1,5-AnG-6-P concentration (as in Figure 2) in the absence of P_i and B is the slope from the plot of (relative velocity of hexokinase I)$^{-1}$ versus 1,5-AnG-6-P concentration in the presence of 6 mM Pi.

a particle in solution is

$$I(s) = \langle |A_a(s) - \rho_S A_S(s) + \delta\rho_b A_b(s)|^2 \rangle \Omega \qquad (2)$$

where $A_a(s)$ is the scattering amplitude from the particle in vacuo, $A_s(s)$ and $A_b(s)$ are, respectively, the scattering amplitudes from the excluded volume and the hydration layer, both with unitary density, $\delta\rho_b = \rho_b - \rho_s$, and the brackets ($\langle\ \rangle$) stand for the average over all particle orientations [Ω is the solid angle in reciprocal space, $s = (s, \Omega)$]. The program uses the multipole expansion of the scattering amplitudes to facilitate the spherical average in eq 2. For solutions containing only monomers, calculated scattering curves (derived from models built as described above) were fit to experimental scattering curves using two free parameters, the excluded volume of the particle, and the contrast of the hydration layer $\delta\rho_b$. For solutions containing mixtures of monomers and dimers, the volume fractions of each component was determined by fitting the experimental data with linear combinations of calculated scattering curves from monomers and dimers, using the program OLIGOMER (D.I.S, unpublished material).

RESULTS

Protein Purity and Circular Dichroism (CD) Spectra. On the basis of SDS−PAGE, wild-type and interface mutant enzymes were at least 95% pure (data not shown). The CD spectra of the wild-type enzyme and the interface mutant enzyme coincide. The addition of Glc-6-P to 1 mM did not influence the CD spectrum of either enzyme (data not shown).

Kinetic Studies. Kinetics parameters for wild-type and mutant hexokinases are identical to within experimental uncertainty (Table 1). The K_m for ATP and the K_i for 1,5-AnG-6-P differ for the wild-type and mutant enzymes by approximately 3 and 4 standard deviations, respectively. The reported standard deviations, however, derive from the random distribution of data about the model for a specific experiment and do not reflect systematic errors, which may arise from variations in stock solutions and different preparations of enzyme. The K_m for ATP of the wild-type enzyme, for instance, has varied from 0.4 to 1.2 mM with an average value of 0.6 mM. Hence, the observed K_m for the mutant is indistinguishable from that of the average for the wild-type enzyme. The K_i for 1,5-AnG-6-P is sensitive to the level of phosphate contamination in the ATP stock solution, as well as the precise determination of ATP concentration. The specific activity of wild-type and mutant enzymes under the conditions of assay here are 61 ± 7 and 60 ± 4 μmol mg^{-1} min^{-1}, respectively. These values are equal to those reported for hexokinase I purified from natural sources. The wild-type and interface mutant enzymes follow the nonlinear competitive mechanism (eq 1, goodness of fit 5%), the two enzymes exhibiting comparable values for K_i and K_{ii}. The high uncertainty in the K_{ii} value is a consequence of the threshold concentration (400 μM) of 1,5-AnG-6-P, which is too low for an accurate determination of a low affinity interaction. Enzyme velocities are very low and subject to significant error at millimolar concentrations of 1,5-AnG-6-P, complicating kinetic assays under conditions, which in principle should allow a more precise determination of K_{ii}. Phosphate relieves inhibition by 1,5-AnG-6-P for wild-type and interface-mutant hexokinases to approximately the same extent. The kinetic parameters for the wild-type enzyme essentially are unchanged from those of the previous study (*18*), except for k_{cat}, which differs slightly due to differences in the buffer system used here (Hepes/sodium acetate, pH 7.8) and in the previous investigation (Tris, pH 7.4).

Models Employed in Calculating X-ray Scattering. Crystal structures of hexokinase I reveal different relative orientations for the first helix of the N-terminal half and the structurally corresponding transition helix, which lies between N- and C-terminal halves. A rotation of 35° about the axis defined in the Materials and Methods and Figure 2 brings the transition helix into alignment with the first helix of the superimposed N-half and results in a monomer with a more compact structure, similar to a bent rod. A rotation of 80° allows the N-terminal half to come in contact with elements of the active site at the C-terminal half (Figure 2). A rotation of 80° creates a new interface, which could transmit the effects of Glc-6-P binding at the N-terminal half to the active site of the C-terminal half. Further positive rotation results in unacceptable steric interactions. Rotations in the opposite direction (hereafter defined as rotations through negative angles) initially produce a more extended monomer (−20° rotation) with no contacts between the N- and C-terminal halves. Further negative rotation leads to bent-rod structures, which are indistinguishable by small-angle scattering from those structures generated by positive rotations. Hence, rotations over the range −20 to 80° sample a full range of global conformations for hexokinase I at the resolution of small-angle scattering data.

Small-Angle X-ray Scattering. Molecular weight determinations by small-angle scattering rely on an accurate determination of hexokinase I concentration. The direct determination of hexokinase I concentration, however, has a 10% uncertainty. This coupled with systematic errors in the acquisition of scattering data for each of the concentration series of Table 2 translates into a 15% uncertainty in the determination of molecular weight. The variations in molecular weight, reported in Table 2, reflect the anticipated level of uncertainty.

Invariants of the scattering curves [the radius of gyration (R_g) and the apparent molecular weight of the macromol-

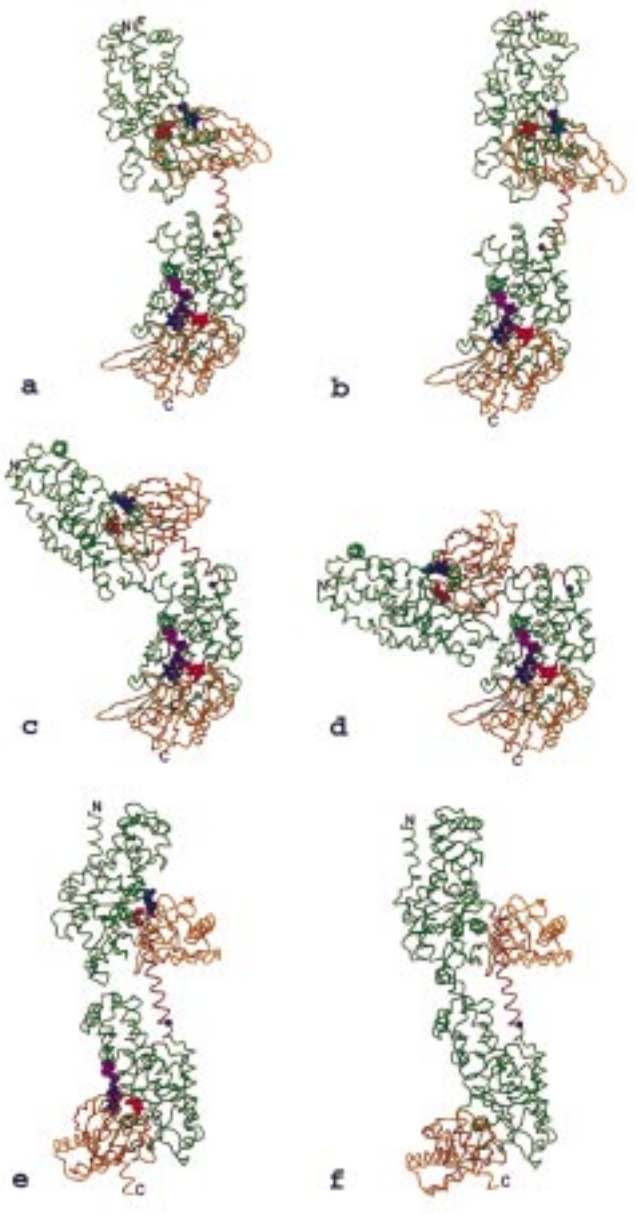

FIGURE 2: Models of hexokinase I used in the analysis of small-angle scattering data. In all images, the C-terminal half is on the bottom, small domains (residues 75−209 and 448−465 of the N-terminal half and residues 523−657 and 896−913 of the C-terminal half) are yellow, large domains (residues 210−447 of the N-terminal half and 658−895 of the C-terminal half) are green, the interdomain helix (residues 448−475) is purple, and ball-and-stick representations of bound glucose, Glc-6-P and ATP are red, blue, and purple, respectively. The ligand binding sites are those observed in crystal structures (*13*, *14*) except for that of ATP which comes from a model (*14*). P_i binds to the N-terminal half at the phosphoryl site of Glc-6-P. (a) A single polypeptide chain from the Glc-6-P/glucose complex (PDB accession label 1HKB), in which both halves are in a closed conformation (*14*). (b) The model corresponding to a rotation angle of −20° (see text for definition of the rotation angle). Note the loss of contacts between the N- and C-terminal halves. (c) The model corresponding to a rotation angle of 35°. The relative orientations of the transition helix (purple) and the corresponding helix (residues 16−27) of the N-terminal half are the same. (d) The model corresponding to a rotation angle of 80°. The N-terminal half is in direct contact with Glc-6-P-binding site of the C-terminal half. (e) A different orientation of the model in (a) to facilitate comparison to the model of (f) where both halves are in an open conformation. Images of hexokinase I drawn with MOLSCRIPT (34) and RASTER3D (35).

Table 2: Experimentally Determined Radii of Gyration, Molecular Masses, and Maximum Intramolecular Distances Calculated from GNOM for Wild-Type and Interface-Mutant Hexokinases[a]

sample[b]	concn (mg/mL)	radius of gyration (nm)	M_r[c] (kDa)	D_{max}[c] (nm)
WT, Glc/Pi	14.4	4.70(0.02)	120	15
	7.2	4.53(0.06)	108	16
	3.6	4.22(0.09)	95	15
WT, Glc/Glc-6-P	14.6	4.57(0.04)	250	15
	7.3	4.38(0.06)	240	14
	3.6	4.61(0.09)	255	15
	0.9	4.53(0.15)	265	15
mutant, .Glc/Pi	16.9	4.18(0.04)	92	15
	8.4	4.65(0.07)	95	15
	4.2	4.34(0.09)	87	15
	1.0	4.43(0.16)	83	15
mutant, Glc/Glc-6-P	14.1	4.32(0.06)	122	15
	7.0	4.37(0.09)	120	15
	3.5	4.35(0.17)	114	15
	1.8	4.37(0.15)	121	15
	0.9	4.34(0.24)	119	15
	0.4	4.23(0.37)	108	14
mutant, Glc/ADP	12.9	4.04(0.06)	102	14
	6.5	4.14(0.07)	112	14
	3.2	4.41(0.12)	130	15
	0.8	4.12(0.23)	121	15

[a] Values in parentheses are standard deviations. [b] Samples contain wild-type (WT) enzyme or interface-mutant enzyme in the presence of Glc/Pi, Glc/Glc-6-P, or Glc/ADP/Mg^{2+}/AlF_3 under conditions provided in the Materials and Methods. [c] Standard deviations of M_r and D_{max} are about 15 and 7%, respectively.

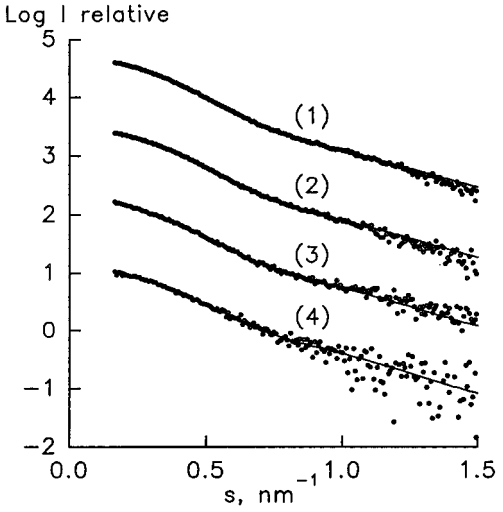

FIGURE 3: Small-angle X-ray scattering from the wild-type enzyme in Glc/Glc-6-P. Curves 1−4 correspond to 14.6, 7.3, 3.6, and 0.9 mg/mL enzyme, respectively. Observed data are represented by circles. Calculated curves (solid lines) are based on a subunit of the Glc/Glc-6-P crystalline complex (rotation, 0°; N- and C-terminal halves closed).

ecule] are consistent with a mixture of monomers and dimers for the wild-type enzyme (Table 2, Figure 3). In contrast, solutions of the interface-mutant enzyme yielded molecular weights and R_g values comparable to those of a monomer for all concentrations and buffers. Quantitative estimates of the composition of the hexokinase mixtures were obtained using OLIGOMER (see Materials and Methods). In the presence of fixed concentrations of Glc-6-P or P_i, the volume fraction of dimers increases with the concentration of the wild-type enzyme (Table 3). P_i stabilizes the wild-type monomer relative to the dimer, whereas Glc-6-P stabilizes the dimer relative to the monomer. A significant portion of

Table 3: Volume Fractions Expressed as Percent Monomers and Dimers of Hexokinase I Present in the Solution on the Basis of Small Angle Scattering Data[a]

sample[b]	concn (mg/mL)	χ[c]	$<M_r>$[d] (kDa)	$<R_g>$[e] (nm)	monomer[f] (%)	dimer[f] (%)
WT, Glc/Glc-6-P	14.6	0.670	196	4.41	3.7(1.0)	96.3(0.8)
	7.3	0.464	192	4.41	8.0(1.6)	92.0(1.2)
	3.6	0.451	182	4.39	17.9(2.6)	82.1(1.9)
	0.9	0.283	179	4.39	20.5(7.8)	79.5(5.5)
WT, Glc/Pi	14.4	1.011	124	4.26	76.2(0.8)	23.8(0.5)
	7.2	0.666	111	4.21	89.4(1.1)	10.6(0.8)
	3.6	0.618	99.9	4.16	100.1(2.0)	−0.1(1.3)
	1.8	0.537	98.7	4.16	101.3(2.5)	−1.3(1.6)
	1.0	0.665	105	4.19	95.4(4.0)	4.6(2.6)
mutant, Glc/Glc-6-P	14.1	0.522	105	4.19	95.1(1.1)	4.9(0.8)
	7.0	0.369	105	4.19	94.7(1.8)	5.3(1.3)
	3.5	0.527	96	4.14	103.6(2.5)	−3.6(1.7)
	1.8	0.364	104	4.18	96.0(2.9)	4.0(2.0)
	0.9	0.346	103	4.18	97.2(4.3)	2.8(3.0)
	0.4	0.251	104	4.18	96.4(11.7)	3.6(8.0)
mutant, Glc/ADP	12.9	0.694	102	4.17	98.3(1.2)	1.7(0.9)
	6.5	0.449	102	4.17	97.6(1.9)	2.4(1.4)
	3.2	0.370	106	4.19	93.9(3.3)	6.1(2.3)
	0.8	0.398	79.9	4.03	120.1(6.4)	−20.1(4.5)

[a] Values in parentheses are standard deviations. [b] Samples contain wild-type (WT) enzyme or interface-mutant enzyme in the presence of Glc/Pi, Glc/Glc-6-P, or Glc/ADP/Mg^{2+}/AlF_3 under conditions provided in the Materials and Methods. [c] Goodness of fit expressed as $\chi^2 = (N-1)^{-1}\Sigma_j[(I(s_j) - I_{exp}(s_j)/\sigma(s_j)]$, where N is the number of data points, $I(s_j)$ the calculated curve, and $I_{exp}(s_j)$ and $\sigma(s_j)$ are the experimental data and their standard deviations, respectively. [d] $<M_r>$ is the volume-fraction, weighted average of the monomer M_r (100 kDa) and the dimer M_r (200 kDa). [e] $<R_g>$ is the volume-fraction, *z*-average of the radii of gyration of the hydrated monomer (4.16 nm) and dimer (4.42). [f] Volume fractions evaluated by OLIGOMER (see Materials and Methods). The program does not restrict the fractions to be within the range 0.0−1.0, hence negative values are possible.

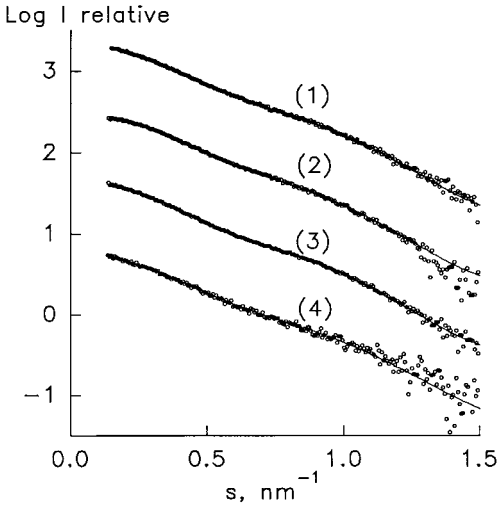

FIGURE 4: Agreement in calculated scattering curves and observed scattering data. Scattering data are from the interface mutant enzyme in Glc/P_i (1), in /Glc/ADP/Mg^{2+}/AlF_3 (2), and in Glc/Glc-6-P (3), and the wild-type enzyme in Glc/P_i. (4). Each curve is offset along the vertical axis in order to facilitate comparisons between observed data (open circles) and the calculated scattering (solid lines) from a subunit of the Glc/Glc-6-P crystalline complex (rotation, 0°; N- and C-terminal halves closed).

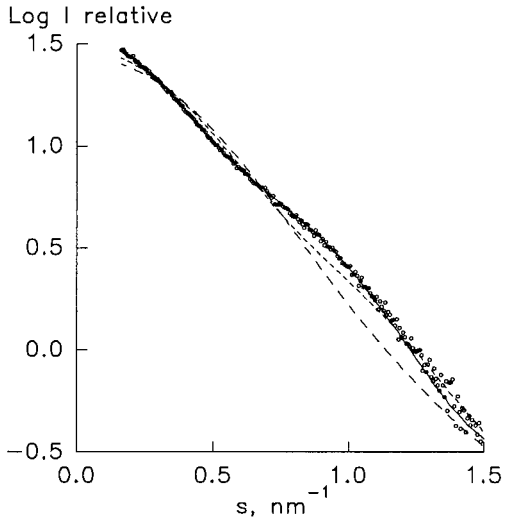

FIGURE 5: Calculated and observed scattering curves from the interface mutant enzyme in Glc/P_i. Observed data are represented by circles. Calculated scattering curves are for the N- and C-halves closed with a rotation of 0° (—), 35° (- - -), and 80° (— —).

the wild-type enzyme is dimeric in the presence of Glc-6-P, even at the lowest enzyme concentration (0.9 mg/mL).

The scattering curves from the interface-mutant enzyme in all solutions were superimposable (Figure 4), the invariants of each curve being indicative of monomeric hexokinase I. Hence, data for the interface-mutant enzyme can be compared directly to calculated scattering curves based on various models for the hexokinase I monomer. The models and scattering curves were generated as described in the Materials and Methods. To test whether the extended conformation of the monomer, observed in the crystallographic dimers, is a consequence of dimerization, models of Figure 2b and Figure 2c were generated using rotation angles of 35 and 80°, respectively. These more compact models, however, gave scattering curves which fit the observed data poorly (Figure 5, Table 4). Calculated scattering curves from extended models, such as those of Figure 2a and 2b, where the rotation angle is either 0 or −20°, provided excellent fits to the observed data (Figure 5, Table 4). The quality of the fit was insensitive to models based on an extended monomer with open and/or closed domains (Figure 2, panels e and f). Models, which fit the observed data well, have in common a rodlike conformation. This rodlike conformation exists in the presence of ligand combinations (Glc/P_i, Glc/Glc-6-P, or Glc/ADP/Mg^{2+}/AlF_3), which should sample all of the anticipated conformational states of hexokinase I.

Table 4: Goodness-of-Fit between Experimental and Calculated Scattering Curves for the Interface Mutant of Hexokinase I[a]

model for calculated data			goodness-of-fit for interface mutant in		
rotation (deg)	C-terminal	N-terminal	Glc/P_i	Glc/Glc-6-P	Glc/ADP/Mg^{2+}/AlF_3
0	open	closed	0.785	0.682	0.565
0	closed	open	0.882	0.740	0.671
0	open	open	0.893	0.780	0.669
0	closed	closed	0.730	0.643	0.536
35	closed	closed	2.11	1.28	1.47
80	closed	closed	3.63	2.01	2.45
−20	closed	closed	0.641	0.462	0.557

[a] Calculated curves are determined from the models of Figure 2, using the program CRYSOL (*29*). The last four entries of Table 4 correspond to models of Figure 2, panels f, a, b, c, and d, respectively. Models for the first two entries of Table 4 are not illustrated here.

The radius of gyration computed from the atomic model of the monomer is 4.1 nm, whereas the experimental values are systematically higher (about 4.2 nm). The increase is due to a higher solvent density in the hydration shell (using CRYSOL, contrasts in the hydration layer $\delta\rho_b$ between 14 e/nm^3 and 38 e/nm^3 for all the fits). These contrasts correspond to bound water of about 1.1 g/cm^3 and to a protein hydration of about 0.23 g of H_2O/g of dry protein, in agreement with results obtained previously for other proteins in solution (*30*).

DISCUSSION

Small-angle scattering data are consistent with appreciable dimer formation for wild-type hexokinase I in the presence of 1 mM Glc-6-P and 2 mM glucose, whereas in the presence of 1 mM P_i and 2 mM glucose, the enzyme is primarily monomeric. The results are in agreement with analytical ultracentrifugation studies of hexokinase I from bovine brain, which indicate enzyme monomers at total protein concentrations of up to 7 mg/mL and a dimer in the presence of Glc-6-P at total enzyme concentrations of 1−1.8 mg/mL (*31*). Either P_i at 10 mM or ATP at 5 mM antagonize dimerization induced by Glc-6-P. Easterby (*32*) reported approximately 9% dimer in the absence of Glc-6-P at total enzyme concentrations of 2.5 mg/mL of hexokinase I from heart. Dimerization is favored by the reduction of ionic strength and pH. Sedimentation coefficients increase for hexokinase I from rat brain in the presence of Glc-6-P at low protein concentration (*12*). P_i reverses the observed increase in sedimentation coefficient. The antagonistic effects of Glc-6-P and P_i putatively demonstrate two conformational states for the monomer, but the same study reported monotonic increases in sedimentation coefficients with increases in total enzyme concentration, a phenomenon not easily reconciled with the existence of a single state of aggregation for the enzyme. Indeed, the sucrose gradient used in the latter study could profoundly stabilize the hexokinase dimer. Polyethylene glycol, for instance, induces crystallization of hexokinase dimers; the effect of polyethylene glycol on the bulk properties of an aqueous solution is not unlike that of a high concentration of sucrose.

In contrast to the wild-type enzyme, the interface mutant remains a monomer at all protein concentrations in the presence of all ligand combinations (Table 3). Furthermore, the mutant enzyme retains a rodlike conformation in solution consistent with Figure 2, panels a, b, e, and f. Small-angle scattering data were insensitive to conformational differences between Glc-6-P- and P_i-bound states of the mutant, with either state explained equally well by models with opened or closed domains (Table 4). No significant change occurs in the radius of gyration of the mutant enzyme in response to antagonistic ligands. Observed changes in sedimentation coefficient for the wild-type enzyme in sucrose density gradients then are not a likely consequence of conformational differences in monomers, but rather may be due to ligand-induced change in the state of aggregation of the wild-type enzyme.

Small-angle scattering data reported here place distinct limits on the conformational changes in monomeric hexokinase I in response to ligand association. Whether it be inhibited by the product, relieved of that inhibition by phosphate, or complexed with putative transition-state analogues (Glc/ADP/Mg^{2+}/AlF_3), the monomer retains a rodlike conformation similar to that observed for a single polypeptide chain of crystallographic dimers. The interface between the N- and C-terminal halves observed in crystal structures involves loop 242−250 of the N-terminal half and residues 796−813 of the C-terminal half (Figure 1). The mutation of Arg801, involved in a salt link between the N- and C-terminal halves of the crystalline dimer, reduces phosphate relief of product inhibition (*18*), a finding which also implicates the interface above in the allosteric mechanism. Hence, existing crystal structures of hexokinase dimers provide a reasonable approximation of the conformation of hexokinase monomers in solution.

Conformational changes associated with the allosteric mechanism of hexokinase I must maintain an extended, rodlike structure. Four kinds of conformational change are possible: (i) rotating the transition helix, as done in the modeling here; (ii) bending the transition helix at its approximate midpoint; (iii) translating the N- and C-terminal halves in opposite directions along the axis of the transition helix; (iv) twisting the N- and C-terminal halves in opposite directions about the axis of the transition helix. Types i−iii above require rotations, bending, and/or displacements of a magnitude that retains an extended molecule with an overall length of 15 nm, whereas any twist (type iv conformational change) would not alter overall length. Conformational changes within either the N− or C-terminal half (such as domain movements between open and closed conformers) are probably of great importance to function, but do not cause a detectable change in the length and/or shape of hexokinase I. So far, crystallographic structures of dimers have revealed only a tendency for the transition helix to bend modestly at its mid-section (*13*).

Small-angle scattering data are inconsistent with any model, whereby the N-terminal half occludes the Glc-6-P pocket of the C-terminal half of the monomer (*4*). For the N-terminal half to block the Glc-6-P pocket of the C-terminal half, the monomer must assume a bent conformation (rotation angle of 80°), which is not observed. Yet, in equilibrium binding experiments, only one Glc-6-P molecule binds to hexokinase I, whereas in crystallographic dimers two molecules of Glc-6-P bind to each polypeptide chain (one each at the N- and C-terminal halves). Hence, some mechanism in the monomer other than occlusion must make the binding of Glc-6-P to the N- and C-terminal halves mutually exclusive. The data here are consistent with a model in which interactions between the N- and C-terminal halves statically perturb one of the Glc-6-P pockets or a model in which the Glc-6-P pockets in the N- and C-terminal halves are coupled by a mechanism of negative cooperativity. Crystal structures of the interface mutant under different states of ligation, could provide more insight regarding interactions between ligand binding pockets of the N- and C-terminal halves. To this end crystals are now available for the interface mutant enzyme in its complex with Glc-6-P, which diffract to 1.9 Å resolution.

REFERENCES

1. Lowry, O. H., and Passonneau, J. V. (1964) *J. Biol. Chem. 239*, 31−42.
2. Katzen, H. M., and Schimke, R. T. (1965) *Proc. Natl. Acad. Sci. U.S.A. 54*, 1218−1254.
3. Schwab, D. A., and Wilson, J. E. (1989) *Proc. Natl. Acad. Sci. U.S.A. 86*, 2563−2567.
4. Wilson, J. E. (1995) *Rev. Physiol. Biochem. Pharmacol. 126*, 65−198.
5. Easterby, J. S., and O'Brien, M. J. (1973) *Eur. J. Biochem. 38*, 201−211.
6. Holroyde, M. J., and Trayer, I. P. (1976) *FEBS Lett. 62*, 215−219.
7. Ureta, T. (1982) *Comp. Biochem. Physiol. B: Comp. Biochem. 71*, 549−555.
8. Manning, T. A., and Wilson, J. E. (1984) *Biochem. Biophys. Res. Commun. 118*, 90−96.
9. Ureta, T. (1975) in *Isozymes III* (Markert, C. L., Ed.) Academic Press, Inc., New York.
10. Ellison, W. R., Lueck, J. D., and Fromm, H. J. (1975) *J. Biol. Chem. 250*, 1864−1871.
11. Fromm, H. J. (1981) in *The Regulation of Carbohydrate Formation and Utilization in Mammals* (Veneziezle, C. M., Ed.) University Park Press, Baltimore, MD.
12. Wilson, J. E. (1973) *Arch. Biochem. Biophys. 159*, 543−549.
13. Aleshin, A. E., Zeng, C., Bartunik, H. D., Fromm, H. J., and Honzatko, R. B. (1998) *J. Mol. Biol. 282*, 345−357.
14. Aleshin, A. E., Zeng, C., Bourenkov, G. P., Bartunik, H. D., Fromm, H. J., and Honzatko, R. B. (1998) *Structure 6*, 39−50.
15. Aleshin, A. E, Fromm, H. J. and Honzatko, R. B. (1998) *FEBS Lett. 434*, 42−46.
16. Mulichak, A. M., Wilson, J. E., Padmanabhan, K., Garavito, R. M. (1998) *Nat. Struct. Biol. 5*, 555−560.
17. Zeng, C., Aleshin, A. E., Hardie, J. B., Harrison, R. W., and Fromm, H. J. (1996) *Biochemistry 35*, 13157−13164.
18. Fang, T.-Y., Alechina, O., Aleshin, A. E., Fromm, H. J. and Honzatko, R. B. (1998) *J. Biol. Chem. 273*, 19548−19553.
19. Bradford, M. M. (1976) *Anal. Biochem. 72*, 248−254.
20. Ferrari, R. A., Mandelstam, P., and Crane, R. K. (1959) *Arch. Biochem. Biophys. 80*, 372−377.
21. Fromm., H. J., and Zewe, V. (1962) *J. Biol. Chem. 237*, 1661−1662.
22. Koch, M. H. J., and Bordas, J. (1983) *Nucl. Instrum. Methods 208*, 461−469.
23. Boulin, C., Kempf, R., Koch, M. H. J., and McLaughlin, S. M. (1986) *Nucl. Instrum. Methods A249*, 399−407.
24. Boulin, C. J., Kempf, R., Gabriel, A., and Koch, M. H. J. (1988) *Nucl. Instrum. Methods A269*, 312−320.
25. Gabriel, A., and Dauvergne, F. (1982) *Nucl. Instrum. Methods 201*, 223−224.
26. Feigin, L. A., and Svergun, D. I. (1987) *Structure analysis by small-angle X-ray and neutron scattering*, Plenum Press, New York.
27. Svergun, D. I. (1992) *J. Appl. Crystallogr. 25*, 495−503.
28. Svergun, D. I. (1993) *J. Appl. Crystallogr. 26*, 258−267.
29. Svergun, D. I., Barberato, C., and Koch, M. H. J. (1995) *J. Appl. Crystallogr. 28*, 768−773.
30. Svergun, D. I., Richard, S., Koch, M. H. J., Sayers, Z., Kuprin, S., and Zaccai, G. (1998) *Proc. Natl. Acad. Sci. U.S.A. 95*, 2267−2272.
31. Chakrabarti, U., and Kenkare, U. W. (1974) *J. Biol. Chem. 249*, 5984−5988.
32. Easterby, J. S. (1975) *Eur. J. Biochem. 58*, 231−235.
33. Harritos, A. A., and Rosemeyer, M. A. (1985) *Biochim. Biophys. Acta 830*, 113−119.
34. Kraulis, J. (1991) *J. Appl. Crystallogr. 24*, 946−950.
35. Merritt, E. A., and Bacon, D. J. (1997) *Methods Enzymol. 277*, 505−524.

BI990523N